Contents list available at IJRED website

International Journal of Renewable Energy Development

Journal homepage: https://ijred.undip.ac.id

Research Article

Analysis of Wake Turbulence for a Savonius Turbine for Malaysia's Slow-Moving Current Flow

Anas Abdul Rahman [a] *, Kumaran Rajendran[a], Ayu Abdul-Rahman[b], Gisrina Elin Suhri[a], Lakshuman Dass[a]

[a]*Mechanical Engineering Program, Faculty of Mechanical Engineering Technology, Universiti Malaysia Perlis, Pauh Putra Main Campus, 02600 Perlis, Malaysia*

[b]*Department of Mathematics and Statistics, School of Quantitative Sciences, Universiti Utara Malaysia, 06010 UUM, Sintok, Kedah, Malaysia*

Abstract. With Malaysia being surrounded by water bodies, tidal energy could be used for energy extraction. While several turbine designs and technologies have been used for tidal energy extraction, information on the use of vertical-axis tidal turbines (VATTs) for shallow-water applications is scarce. However, implementing horizontal-axis tidal turbines (HATTs) is not feasible due to Malaysian ocean depths. Hence, examining the wake-flow characteristics of VATTs in a shallow water-working environment in Malaysia is essential. The wake turbulence of the Savonius turbine model was compared with that of a hypothetical 'actuator' cylinder, a VATT representation. Subsequently, the wake turbulences of a Savonius turbine model in static and dynamic simulations were compared to understand the flow distinction. Compared with that exhibited by the hypothetical actuator cylinder of 2.5 m, the hypothetical actuator cylinder of 5 m exhibits greater velocity deceleration. Additionally, the modelled Savonius turbine exhibits significantly more deceleration than that exhibited by the hypothetical actuator cylinder. Finally, the analysis of the static model of the Savonius turbine shows deceleration that is greater than that of the dynamic model.

Keywords: Shallow depth, marine energy, velocity recovery, cross flow turbines, vertical-axis turbine

Received: 27th April 2022; Revised: 5th July 2022; Accepted: 18th July 2022; Available online:1st August 2022

1. Introduction

Every year, due to increasing populations and economic growth, energy production and consumption drastically increase (Daniel & Nicklas, 2013). The global consumption of electricity is projected to increase by 2.5% per year between 2008 and 2035, from 16,819 to 32,922 TWh (Satrio *et al.,* 2016). Malaysia generates more than 80% of its energy from non-renewable sources, such as fossil fuels and coal (Yaakob *et al.*, 2013), which indicates its significant reliance on fossil fuels. As reported in the Malaysia Energy Statistics Handbook 2020, energy consumption in Malaysia has increased drastically, from 25,558 ktoe in 1998 to 64,658 ktoe in 2018 (Energy Commission of Malaysia, 2020). Interestingly, over this period, energy consumption from petroleum products has decreased by almost 20%, partly due to the large increase in natural gas usage.

Renewable energy resources, such as solar, wind, biomass, and ocean energy, must be used to address this issue. Due to its geographical location, Malaysia is blessed with this type of energy, rendering the use of ocean energy a greater concern. European countries are currently at the forefront of the research and development of marine energy, which has attracted considerable interest from industries, governments, and academia alike (Magagna & Uihlein, 2015).

There are various options for extracting energy from the ocean, classified as wave energy (Musa *et al.*, 2020), tidal barrage (Neill *et al.*, 2021), salinity gradient power (Jung *et al.*, 2022), ocean thermal energy conversion (OTEC) (VanZwieten et al., 2017), and tidal turbine (Marsh *et al.*, 2021). Tidal turbines are considered a cost-effective alternative to harness ocean resources compared to wave energy, OTEC, and salinity gradient power (Chong & Lam, 2013). The tidal turbine generates electricity due to ocean–tide variations (Rahman *et al* 2019). Tidal forces generated by the sun and moon create tidal motions according to the earth's rotation (Faez Hassan *et al.*, 2012).

Common tidal turbine technologies can be classified as vertical-axis tidal turbines (VATTs), horizontal-axis tidal turbines (HATTs), and oscillating hydrofoils. Examples of VATT devices (commercially available and in prototype stages) are the Kobold, Darrius, Savonius, and Gorlov turbines, while SeaGen and OpenHydro are the examples of HATT. Likewise, stingray is an example of an oscillating hydrofoil device.

* Corresponding author:
Email: anasrahman@unimap.edu.my (A.A. Rahman)

https://doi.org/10.14710/ijred.2022.45985
ISSN: 2252-4940/© 2022.The Author(s). Published by CBIORE

Lim and Koh (2010) were among the first to conduct an analytical assessment of marine energy potential in Malaysia based on the assumption of employing twin HATT at selected sites. Abdullah *et al*. (2021) also selected HATT (with a rated capacity of 10 kW) to simulate the optimal configuration of a small-scale hybrid device utilising solar- and tidal-power systems for usage in rural areas. A similar endeavour by Tan, Kirke, and Anyi (2021) employed a horizontal turbine to create a prototype for remote electrification purposes. Meanwhile, Behrouzi *et al.* (2016) emphasised that deploying conventional tidal turbines in Malaysia was not an option due to the low-current speed observed in Malaysian waters. In the same paper, they also highlighted several studies by researchers from the Universiti Teknologi Malaysia that focused on novel designs of VATT to improve the performance and efficiency of the device in a slow-moving flow environment. Equally important, Kirke (2019) provided an honest assessment of the issues regarding hydrokinetic turbine deployment in shallow-water regions (e.g., rivers). He argued that most hydrokinetic devices on the market, either VATT or HATT, were designed to be operated at a current velocity of ~3 m/s. This could be a major obstacle to the mass deployment of these devices in rural areas or shallow-water regions, including Malaysia, where the average flow speed is ~1 m/s.

However, a comprehensive review on the use of the Savonius turbines for river-based extraction in Malaysia has been conducted by Badrul Salleh, Kamaruddin, and Mohamed-Kassim (2019), discussing various parameters affecting the performance of the Savonius turbines. Maldar, Ng, and Oguz (2020) also conducted a similar study that highlighted the limitations of the Savonius turbine in extracting energy in a low-velocity environment. In addition, several other studies involving the optimisation of the Savonius tidal device, both numerically and experimentally, have also been conducted. Kumar *et al*. (2020) investigated the influence of the number of stages on the performance of the twisted-blade Savonius device, reporting a maximum power coefficient value of 0.44 for a double-stage turbine with a tip-speed ratio of 0.9. Meanwhile, Alipour *et al*. (2020) reported a significant gain in the maximum power coefficient of a Savonius turbine design that employed a parabolic-shaped blade instead of the commonly used arc design. However, Alizadeh, Jahangir, and Ghasempour (2020) demonstrated that the maximum generated power of a conventional Savonius turbine could be increased by 18% by incorporating a barrier in the design.

When considering a turbine for applications, numerous things must be considered, including the clearance needed, ocean current, turbine effectiveness at a certain ocean current, and cost. HATT is inappropriate for deployment in most Asian countries, such as Malaysia, as the ocean depth is between 20 and 30 m. By contrast, VATT is the most suitable type of a turbine based on Malaysia's geographical constraints and current speed (Azrulhisham *et al.,* 2018; Faez Hassan *et al*., 2012; Maldar *et al.,* 2022). Additionally, the current velocity due to tidal variation in Malaysia is minimal because of the geographical limitations. Moreover, as most research on vertical-axis turbines focus more on wind turbine applications, there are some limitations in terms of data and knowledge with respect to the VATT characteristics, specifically for application in shallow water.

Due to the device's clearance requirements for the top and bottom of the water column, VATT is the best type of turbine to be deployed in shallow water (Roberts *et al*., 2016). Particularly, HATT may also cause complications if used at a shallow depth due to the movement of sediments. While most experts have been exploring the best technique to enhance the efficiency of the existing turbine design, most past research focused on the HATT technology. Thus, a comprehensive study must be conducted to improve the conventional VATT design.

Therefore, this study seeks to bridge the gap in research related to Malaysia's marine renewable energy environment by analysing the flow characteristics of the VATT. The first investigation compared the Savonius turbine models' wake characteristics to those of a hypothetical VATT 'actuator' cylinder. Then, in the second investigation, the wake characteristics of a Savonius turbine model were studied in static and dynamic simulations. To illustrate a better understanding of the wake properties of the Savonius turbine, outputs from this study were compared against published data. As discussed, in the case of tidal streams, this study considers two primary types of turbines, namely the HATT and VATT. Table 1 presents the differences between the two types of the tidal devices.

There are a few well-known VATT designs produced commercially in the market; each turbine design is unique in terms of its performance and specifications. Fig. 1 shows the types of VATT turbines. Meanwhile,

Table 2 highlights the devices' specifications.

Table 1
Distinction between HATT and VATT

HATT	VATT
Maintenance is needed at a higher sea level.	There is little maintenance needed.
HATT is more efficient since it can extract a significant quantity of energy.	VATT is inefficient since it can extract less energy.
HATT is only suited for ocean currents of moderate to high strengths.	VATT is suited for ocean currents of low, moderate, and high strength.
It is challenging to install HATT.	VATT is quite simple to set up.
HATT produces a significant amount of noise.	VATT produces a negligible amount of noise.

Source: Satrio, Utama, and Mukhtasor (2016)

Table 2
VATT variations and their specifications

VATT type	Current velocity	Efficiency
Darrieus Turbine	1.10 m/s	20.00%
Helical Savonius Turbine	1.50 m/s	35.00%
Kobold Turbine	1.80 m/s	23.00%
Davis Turbine	2.50 m/s	30.00%

Source: Yaakob *et al.* (2013)

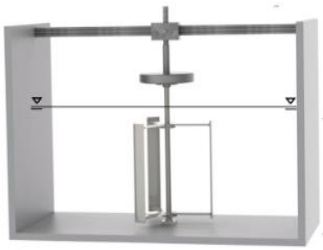

(a) Darrieus Turbine (Priegue & Stoesser, 2017)

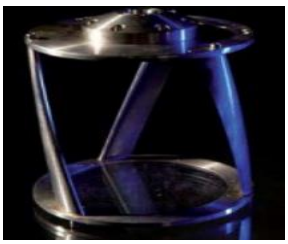

(b) Helical Savonius Turbine (Anderson *et al.*, 2011)

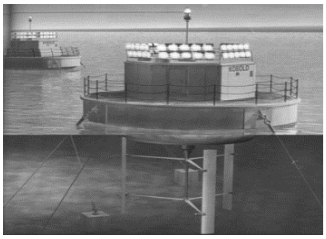

(c) Kobold Turbine (Coiro et al., 2005)

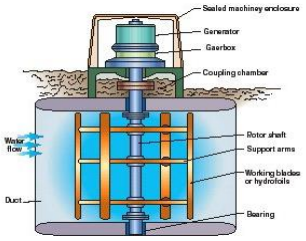

(d) Davis Hydro Turbine (Davis, 2001)

Fig. 1 Different vertical-axis tidal turbine designs

Table 3
Current speeds at several sites around Peninsular Malaysia

Sites	Maximum speed (m/s)	Current range (m/s)
One Fathom Bank	1.18	0.41–0.77
Off Raleigh School	1.13	0.46–0.77
Tanjung Segenting	1.03	0.41–0.67
Pulau Tioman	0.59	0.05–0.29

Source: Yaakob, Rashid, and Mukti (2006) and Maldar *et al.* (2022)

Table 3 highlights the current speeds for several locations around Peninsular Malaysia as presented by Yaakob, Rashid, and Mukti (2006) and Maldar *et al.* (2022) Malaysia's average ocean-current velocity can be approximated to be 0.56 m/s. The Savonius turbine has been recommended as the best device to be deployed (O. B. Yaakob *et al.*, 2013). Thus, here, we selected the Savonius turbine with the current flow set to 0.6 m/s.

2. Methodology

2.1 Governing equations

The Reynolds-averaged equations of mass conservation are described in Equation. (1) while momentum conservation is presented in Equation (2).

Mass conservation

$$\frac{\partial U_i}{\partial x_i} = 0 \tag{1}$$

Momentum conservation

$$\frac{\partial(\rho U_i)}{\partial t} + \frac{\partial(\rho U_i U_j)}{\partial x_j} = -\frac{\partial P}{\partial x_i} + \frac{\partial}{\partial x_j}\left[\mu\left(\frac{\partial U_i}{\partial x_j} + \frac{\partial U_j}{\partial x_i}\right)\right] + \frac{\partial}{\partial x_j}\left(-\rho\overline{u_i' u_j'}\right) + \rho g_i + S_i \tag{2}$$

Here, U_i (i = u, v, w) is the velocity of water averaged over time t, x_i (i = x, y, z) is the distance, ρ is the density of water, P is mean pressure, μ is viscosity, $-\rho\overline{u_i' u_j'}$ is the Reynolds stress which must be resolved with a turbulence model, u' is an instantaneous velocity fluctuation over time from the mean velocity, g_i is the gravitational acceleration component, and S_i is an added source term to the i = x, y, or z momentum equation.

2.1.1 Energy conversion

The power generated by the tidal stream current is (Satrio *et al.*, 2016):

$$P = 0.5A\rho v^3 \tag{3}$$

where ρ (kg/m^3) is the fluid density, A (m^2) is the turbine rotor area, and v (m/s) is the fluid velocity.

HATT and VATT have different cross-sectional areas (A). The cross-sectional area of HATT will be:

$$A = 0.5D^2\pi \tag{4}$$

For the VATT, it will be the height (H) multiplied by the diameter (D) of the rotor, as shown in Equation (5).

$$A = DH \tag{5}$$

Due to certain losses, tidal current can extract only a fraction of this energy, and Equation (3) can be modified as follows (Faez Hassan *et al.*, 2012):

$$P = 0.5V^3 C_p A\rho \tag{6}$$

where C_p = coefficient of power.

Due to the computational constraints, the conventional k-epsilon model was employed in this research as it is the most frequently used CFD technique for simulating mean flow characteristics under turbulent

flow circumstances (Scott-Pomerantz, 2004). It is a two-equation model that provides a general description of turbulence using two transport equations that account for historical effects, such as the diffusion of turbulent energy (Kuzmin *et al*., 2007). The k-epsilon model is a realistic implementation helpful when dealing with wall treatment. The numerical execution of turbulence models includes numerous computational components and variables, whereby each component or variable may significantly impact the quality of the simulation's output (Kuzmin *et al*., 2007). When analysing turbulent flow within a pipe, one may estimate the turbulent intensity using the following formula:

$$I = 0.16 Re_{DH}^{\frac{1}{8}} \quad (7)$$

where Re_{DH} = Reynolds number associated with a pipe with a hydraulic diameter of DH.

Turbulent dissipation can be calculated using the following formula (Johnson, 2015):

$$\varepsilon = \frac{C_{\mu}^{\frac{3}{4}} k^{\frac{3}{2}}}{l} \quad (8)$$

where C_{μ} = constraint for the turbulence model, typically set to 0.0009, k = turbulence energy, and l = turbulence length.

2.2 Model configuration

Upon deciding that the Savonius would be a viable turbine to be deployed in shallow water, this study focuses on the influence of turbine designs on wake turbulence. Then, two factors were selected for analysis: (i) the overlap ratio and (ii) the stacking of the turbine. The turbine model used in this analysis is 2.5 m in diameter and 5 m in height, giving a 2:1 aspect ratio (AR). The overlap ratio parameter was analysed for values of 0, 0.1, 0.2, and 0.3 since they were also employed in several other studies by O. Yaakob, Tawi, and Sunanto (2010), Badrul Salleh, Kamaruddin, and Mohamed-Kassim (2019), and Suhri *et al*. (2022). Meanwhile, the stacking parameters of the turbine were analysed for single, double, and triple stacking. According to Menet (2004) and Mahmoud *et al*. (2012), a Savonius turbine with end plates provides superior hydrodynamic performance. Therefore, the Savonius turbine used in this study features end plates.

The geometry was created using CATIA software, and the analysis was done using ANSYS Fluent. The open channel's border condition or domain is based on Hoe (2019) earlier technical study. Seawater has a density of 1023 kg/m^3 and dynamic viscosity of 0.00092 Ns/m^2. The density and viscosity of seawater were calculated using Malaysia's average ocean temperature of 27 °C (Bakri 2020). The device's top and bottom clearance were set at 5 to 15 m from the ocean's surface and the lowest depth (Fig. 2). As a result, the domain for ANSYS Fluent is limited to 30 m.

The boundary conditions specified in the ANSYS software are depicted in Fig. 3. The diagram depicts the turbine from the top. The front and sides are 15 m apart, while the back is 75 m long to reveal a fully developed wake turbulence region. The Savonius turbine diagram employed in this study is shown in Fig. 4. The model's AR was set at 2. The AR was calculated using the following formula (Mahmoud *et al*., 2012):

$$\alpha = HD^{-1} \quad (9)$$

where α is the turbine's AR, H is the turbine's height, and D is the turbine's diameter.

The turbine's overlap ratio was calculated by dividing the overlap distance (e) by the bucket's diameter (d), where d was set at 1.25 m. The turbine's overlap ratio could be determined using the following equation (Roy & Saha, 2013):

$$\beta = ed^{-1} \quad (10)$$

where β is the turbine's overlap ratio, e is the distance between the two buckets that overlap, and d is the single bucket diameter.

The turbine model would be identical for single, double, and triple stacking, with each stack having a unique 90 degree-phase angle. The model parameters are described in detail in Table 4, considering the average depth of Malaysia's open water and the clearance needed for the turbine placement, as illustrated in Fig. 2.

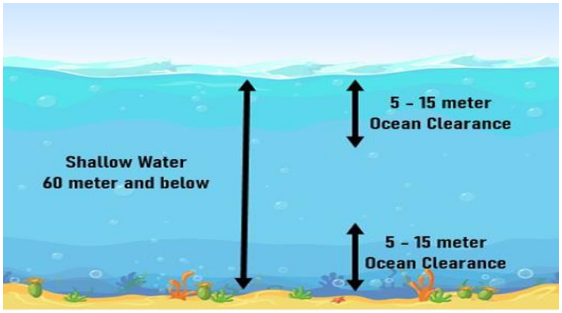

Fig. 2 Shallow-water conditions and ocean clearance needed

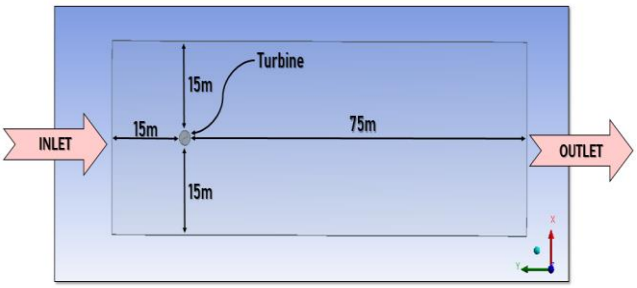

Fig. 3 Domain that was employed in this study from the top view

Table 4
Savonius turbine-model parameters

Parameters of the model	Dimensions
Height of turbine, H	5 m
Diameter of turbine, D_h	2.5 m
Thickness of a bucket	0.05 m
Thickness of the end plates	0.1 m
Rotor's diameter, d	1.25 m

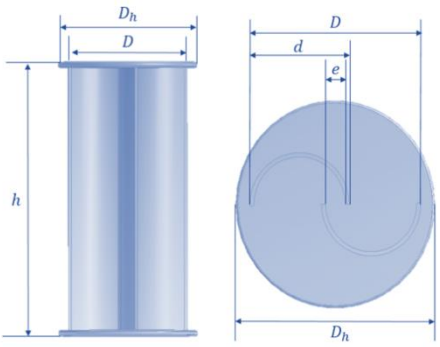

Fig. 4 Diagram of the Savonius turbine design used in this study

2.3 Mesh generation

Mesh generation is critical for generating accurate outcomes in any numerical modelling. A smaller mesh element size may provide a more precise outcome. However, the time required to generate a highly refined mesh is longer. Hence, a grid dependency study was conducted to find the balance between accuracy and the computational resources available. Table 5 summarises the element sizes tested in this study with their corresponding number of nodes and elements. The smallest element tested was set at 1.5 m, while the largest element size was 3.5 m. The number of elements varies significantly from very fine (1,829,624) to very coarse setup (467,634). The velocity profile at 12D (i.e., 12 multiplied by the diameter of the turbine) was observed to analyse the influence of element size on the simulation output.

Fig. 5 shows the velocity profiles for all refinement values at 12D downstream of the device, where very fine and fine element sizes demonstrate output values close to one another. Additionally, Fig. 6 illustrates the observed maximum velocity values for each refinement type at mid-point position 12D downstream of the device. This figure shows the differences between very fine and very coarse-grid sizes are minimal at only 0.062 m/s, indicating that the model output did not differ much based on the tested element size. Hence, considering the computational resources available and the time taken to run the model, the 2-m element size was selected and employed in this study.

The mesh refinement area was focused around the turbine. However, a finer mesh may be produced using a high-performance computer. Fig. **6** Maximum velocity at a mid-point position 12D value of the downstream of the turbine

Table 6
Mesh configuration in ANSYS Fluent

Mesh configuration	
Element Size	2 m
Max Size	2 m
Min Size	~0.02 m
Smoothing	High

Table 7
ANSYS simulation setup

Simulation setup	
Viscous model	Standard k-epsilon
Material	Seawater
Density	1023 kg/m^3
Viscosity	0.00092 Ns/m^2
Solution method	Second order upwind

highlights the mesh configuration employed in this research work. The mesh generated based on the results from the grid dependency study is illustrated in Fig. 7. In accordance with the mesh statistics, the total number of nodes and elements produced by the configuration was 223,125 and 1,200,818, respectively.

Table 5
Grid sensitivity study

Type of refinement	Element size (m)	No. of nodes	No. of elements
1 (very fine)	1.5	359,623	1,829,624
2 (fine)	2.0	223,125	1,200,818
3 (medium)	2.5	159,071	670,871
4 (coarse)	3.0	135,484	536,791
5 (very coarse)	3.5	123,086	467,634

ANSYS Fluent software was used to perform the simulation. Two distinct techniques may be used to generate wake turbulence: (i) the dynamic mesh method and (ii) the sliding mesh method. The motion of a sliding mesh requires a constant rotational velocity. Conversely, the dynamic mesh generates a new angular velocity depending on the pressure and viscous forces operating in the area. In this study, it is assumed that the rotational velocity is constant. Therefore, the wake result was obtained using the sliding mesh method. Table 6
Mesh configuration in ANSYS Fluent

Mesh configuration	
Element Size	2 m
Max Size	2 m
Min Size	~0.02 m
Smoothing	High

Table 7 lists the simulation parameters employed in the study.

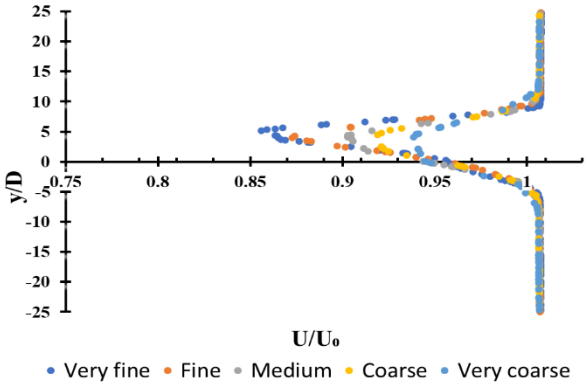

Fig. 5 Velocity profile for all refinements tested at a position of 12D value of downstream distance

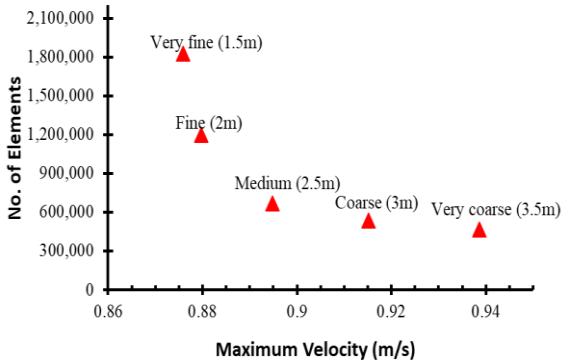

Fig. 6 Maximum velocity at a mid-point position 12D value of the downstream of the turbine

Table 6
Mesh configuration in ANSYS Fluent

Mesh configuration	
Element Size	2 m
Max Size	2 m
Min Size	~0.02 m
Smoothing	High

Table 7
ANSYS simulation setup

Simulation setup	
Viscous model	Standard k-epsilon
Material	Seawater
Density	1023 kg/m^3
Viscosity	0.00092 Ns/m^2
Solution method	Second order upwind

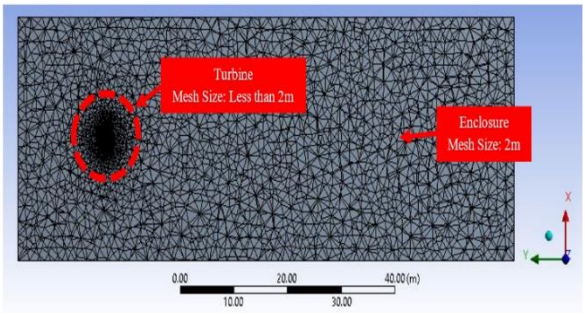

(a) Top View

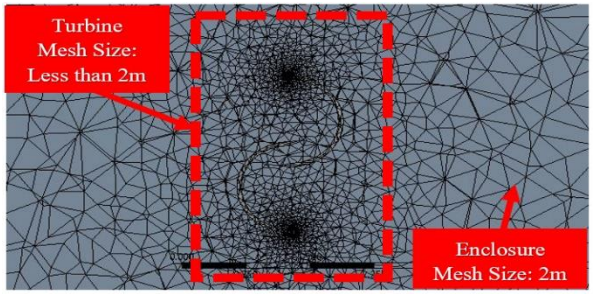

(b) Close-up view

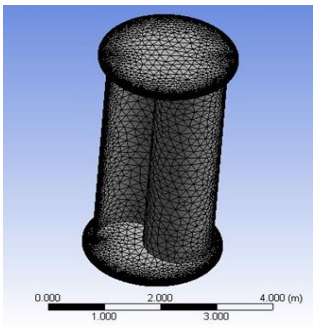

(c) Mesh of turbine without enclosure

Fig. 7 Mesh outcomes according to the selected configuration

The extraction point of the wake turbulence is commonly known as the slicing point. The extraction point is where the reading of the wake turbulence data is obtained. Three extraction points were selected for this study—5D, 7D, and 9D, where D refers to the downstream position from the turbine and the numbers represent the extraction location. For example, 5D suggests that the distance from the turbine downstream is 5 m × 2.5 m of the turbine diameter, equivalent to 12.5 m away from the turbine. Fig. 8 and Table 8 illustrate the distance for each extraction point from the turbine.

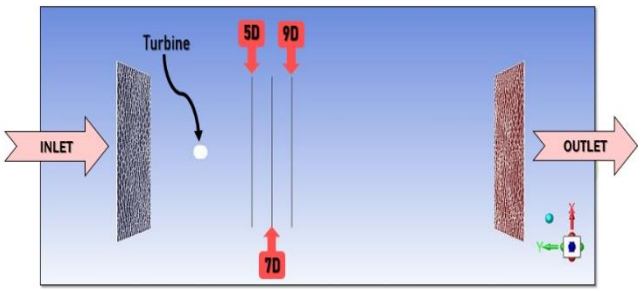

Fig. 8 Extraction points for 5D, 7D, and 9D

Table 8
ANSYS simulation setup

	Distance from the turbine (-Y)
5D	12.5 m
7D	17.5 m
9D	22.5 m

3. Results and Discussion

Results from the static and dynamic simulations are presented in this section, focusing on the wake turbulence of the turbine. Fig. 9 illustrates the design for three different geometries used in the first analysis. The first validation compared the VATT hypothetical actuator cylinder design from Bakri (2020) to the Savonius turbine design created for this study. The cylindrical design by Bakri (2020) was replicated using the previously described parameters to compare the wake turbulence produced by the two distinct geometries. The single-stage Savonius turbine with a 0.2 overlap ratio was selected for validation. The seawater velocity was set to 1 m/s to follow the current velocity employed by Bakri (2020). As Bakri's hypothetical actuator cylinder was 5 m in height and diameter, the

dimensions of the replicated design did not correspond to the same AR of the device designed for this project.

The initial comparative analysis was between a 5 m diameter cylinder (based on work by Bakri (2020)) and a 2.5 m diameter cylinder. The difference in AR between the 5 m and 2.5 m diameters is 1 and 2. The turbine AR is calculated by dividing the height of the turbine over the diameter of the turbine.

The validation was conducted between the two distinct hypothetical actuator cylinder sizes to determine how the device size can affect the turbine's wake turbulence and which design shows the fastest recovery on the velocity. Fig. 10 (a) and (b) demonstrate the contour plot of the two cylindrical objects with distinct ARs.

According to simulation results, the downstream velocity reduction for the cylinder with a diameter of 5 m is greater than that for the cylinder with a diameter of 2.5 m. Thus, it can be concluded that as the diameter increases, the time taken by the cylinder to recover from the flow mixing downstream of the object will be longer. By contrast, for the 2.5 m diameter, the wake recovery contour is shorter, suggesting a quicker flow recovery.

The need for rapid recovery of the flow velocity to the ambient speed is essential for shallow-water applications since it may free up space under the sea and even allow for the placement of more turbines. Hence, the design of a hypothetical actuator cylinder with a 2.5 m diameter is compared to the Savonius turbine design used in this study, having the same diameter, as illustrated in Fig. 10 (c).

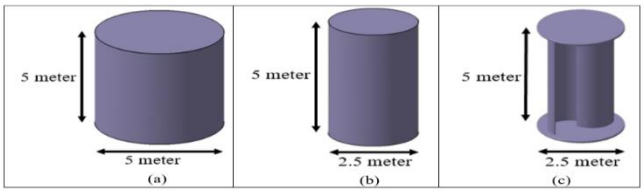

Fig. 9 Geometry design for the first investigation. (a) Hypothetical actuator cylinder with 5 m diameter based on a previous study by Bakri (2020) (b) Hypothetical actuator cylinder with 2.5 m diameter and (c) Savonius turbine with 2.5 m diameter

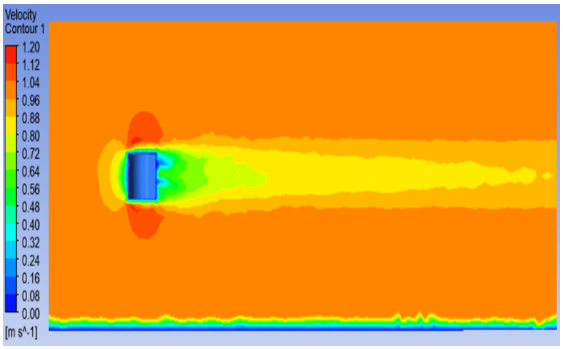

(a) 5 m diameter hypothetical actuator cylinder

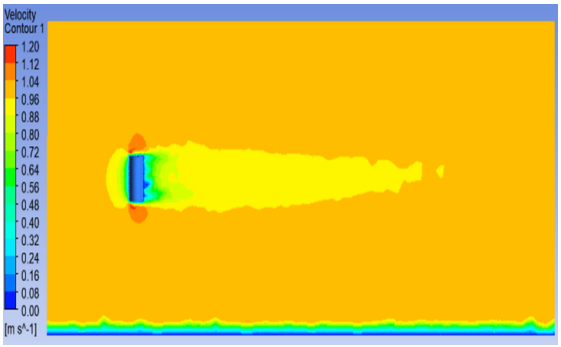

(b) 2.5 m diameter hypothetical actuator cylinder

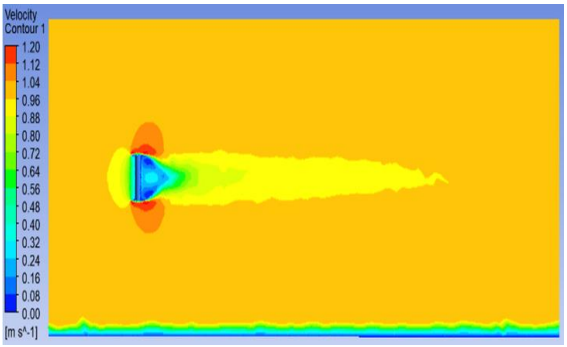

(c) 2.5 m diameter single-stage Savonius turbine with overlap ratio of 0.2

Fig. 10 Comparison of the velocity-wake differences for three devices with distinct geometrical parameters (side view)

The Savonius turbine's design parameters used in this study are comparable to those employed in the simulation study by Bakri (2020), the only distinction is the geometrical shape. The blue contour indicates 0 m/s, whereas the red contour represents 1.2 m/s, as seen in the simulation results. Furthermore, the following comparison between the flow of the Savonius turbine's wake and the hypothetical actuator cylinder's wake indicated that the Savonius turbine had a faster rate of flow recovery. This rate is related to the geometrical form, which is influenced by the slow-current movement. Seawater flows more easily in a cylindrical shape, and thus, the fluid recovers its speed much quicker than in the Savonius turbine design

In the case of a Savonius turbine, fluid fluctuations on the upstream surface of the Savonius rotor would result in a velocity slowdown and a longer recovery time. Fig. 11 shows two different fluid circulations based on two distinct geometrical shapes. It is critical to understand the effect of the turbine's real design on the wake turbulence while planning the deployment of the devices in the sea. This understanding is to ensure that the devices can operate effectively, which was further emphasised by Aliferis, Bracchi, and Hearst (2019), who noted that the wake behaviour is critical for installing numerous turbines in a limited area. The percentage deviation data presented in

Table 9 are based on verified data. Based on the above description, the wake turbulence differences for the three distinct geometries are plotted for 5D, 7D, and 9D, as illustrated in Fig. 12. Note that 'Previous Study X' in the figure legends corresponds to the results from the study conducted by Bakri (2020).

The plots in Fig. 12 for 5D, 7D, and 9D demonstrate excellent mechanics of the trend. The trend is the same for

5D, 7D, and 9D; the only variation is in the velocity changes. The percentage divergence between a hypothetical actuator cylinder with a diameter of 5 m designed by Bakri (2020) and that designed in this study is shown in

Table 9. Similarly, the percentage difference between a 2.5 m diameter cylinder and the Savonius turbine design is depicted in the same table.

The data of percentage deviation was computed using data collected from the device's mid-point location behind the given interval. According to Fig. 12, a cylinder with a diameter of 5 m has a greater velocity reduction than a cylinder with 2.5 m in diameter. As such, it takes longer for the former to recover. The wake turbulence mismatch between the 2.5 m diameter cylinder and the 2.5 m diameter Savonius turbine design further supports the previous reasoning. The Savonius turbine design has a greater velocity deceleration than the cylinder with a diameter of 2.5 m, as depicted in Fig. 11. As a result, the wake recovery for the Savonius turbine design at the freestream flow speed is much slower.

The plots presented show that the Savonius turbine design exhibit a greater velocity drop than a 2.5 m hypothetical actuator cylinder. Therefore, if a 5 m diameter Savonius turbine is designed, the velocity deficit across the 5 m diameter hypothetical actuator cylinder will undoubtedly grow. As such, it will take longer for the cylinder to regain its ambience velocity.

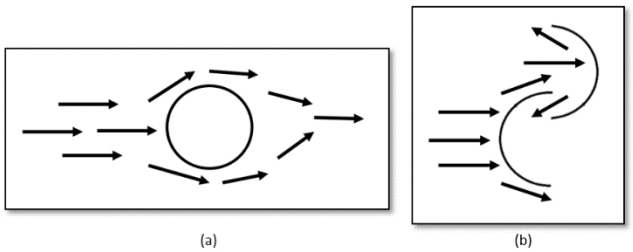

Fig. 11 Circulation pattern of flow around two distinct geometries (a) Cylindrical shape (b) Savonius turbine rotor design

Table 9
Velocity differences observed between two distinct sets of geometrical shapes downstream of the mid-point position of the devices

Compared data	Percentage of deviation		
	5D	7D	9D
Hypothetical actuator cylinder (5 m vs 2.5 m diameter)	8.11	5.91	4.26
Hypothetical actuator cylinder (D = 2.5 m) vs actual Savonius turbine design (D = 2.5 m)	1.62	3.23	2.13

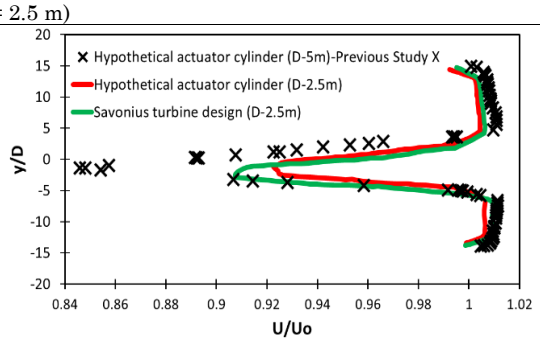

(a) 5D

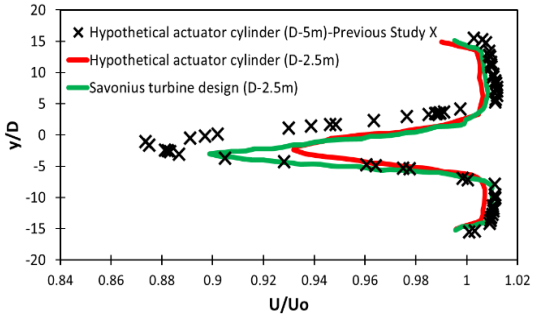

(b) 7D

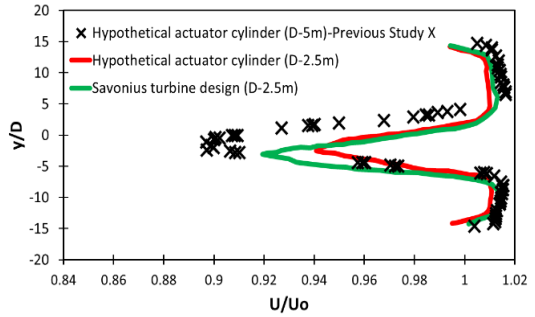

(a) 9D

Fig. 12 Validation of the wake turbulence difference between a hypothetical actuator cylinder of 5 m diameter, a 2.5 m diameter hypothetical actuator cylinder, and a 2.5 m diameter Savonius turbine design

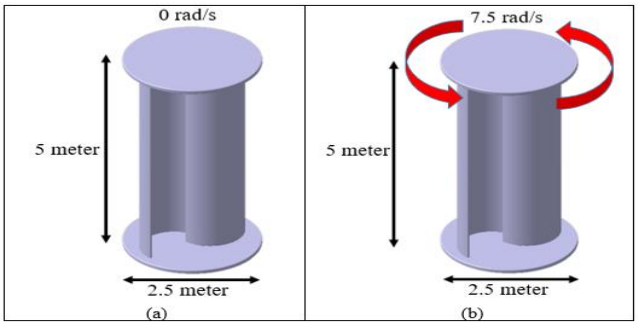

Fig. 13 Geometry setup for (a) static and (b) dynamic simulation of Savonius turbine

Aliferis, Bracchi, and Hearst (2019) state that even if the Savonius turbine has a greater velocity slowdown owing to the rotor blockage, which influences the fluid passing through the turbine, the Savonius turbine's drag force will rise. Due to the tiny gaps through which fluid may enter the Savonius turbine, the blocking effects can be maximised even at a low rotational speed. To conclude, the plots and data for the percentage of deviation proved that utilising a 2.5 m diameter rather than a 5 m diameter would result in a quicker wake recovery velocity.

Furthermore, static and dynamic models were also used to investigate the wake turbulence downstream of the turbine (Fig. 13). The rotation velocity will be absent for the turbine in the static model. By contrast, the dynamic model is imposed with a rotational velocity of 7.5 rad/s. The turbine design was assumed to rotate at a steady velocity of 7.5 rad/s, and the value was obtained based on the previous experiment research by Khan *et al.* (2009). This study aims to determine how the turbine's rotation could impact the wake turbulence

downstream of the device by analysing data from the 5D, 7D, and 9D positions. In both simulation studies, the seawater velocity was set at 0.6 m/s. Both designs were verified using a 0.2 overlap ratio Savonius turbine. The generated contours of the wake turbulence are shown in Fig. 14 (a) and (b) for the static and dynamic simulations, respectively. Moreover,

Table 10 illustrates the difference in the percentage deviation between the static and dynamic simulations for a single-stage Savonius turbine.

Additionally, Fig. 15 demonstrates an excellent result in terms of velocity deficit trend for both simulations. According to the chart of 5D, the seawater velocity in static simulations drops to 0.512 m/s, and the velocity in dynamic simulation drops to 0.521 m/s. The percentage deviations for 5D, 7D, and 9D are 1.73%, 2.04%, and 2.53%, respectively, as mentioned in

Table 10.

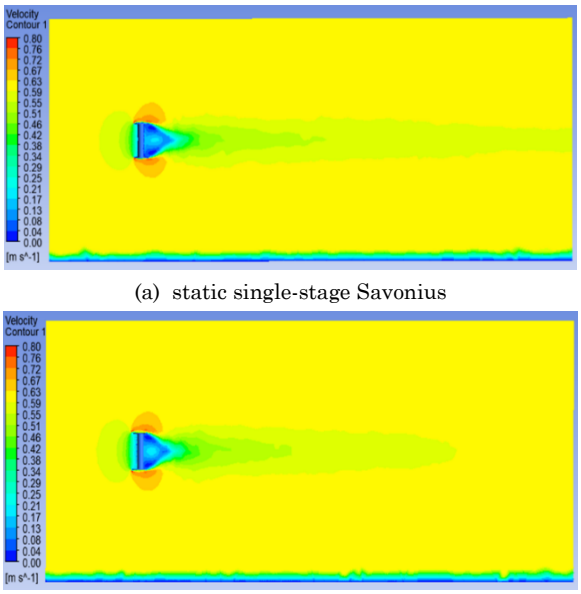

(a) static single-stage Savonius

(b) dynamic single-stage Savonius

Fig. 14 Comparison of the velocity-wake differences for the static and dynamic simulations of the Savonius turbine with an overlap ratio of 0.2 (side view)

Table 10
Comparison in percentage deviation between the static and dynamic simulations of a single-stage Savonius turbine with a 0.2 overlap ratio

Static vs dynamic simulations		
Percentage of deviation (%)	5D	1.73
	7D	2.04
	9D	2.53

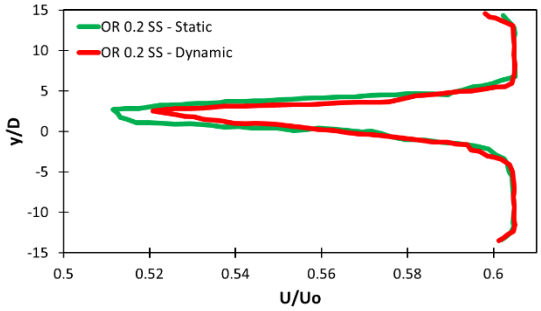

(a) 5D

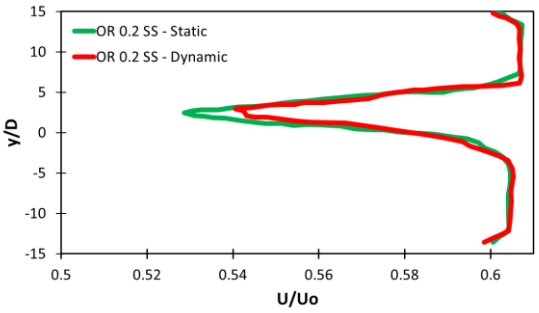

(b) 7D

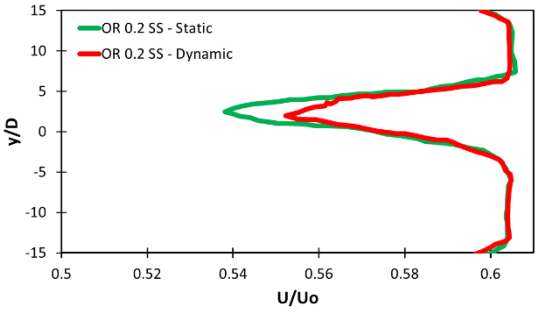

(c) 9D

Fig. 15 Validation of the difference in wake turbulence between the static and dynamic simulations of a single-stage Savonius turbine with an overlap ratio of 0.2

In conclusion, since the turbine will rotate in a real-world application, the velocity recovery will almost certainly be rapid. However, this condition also depends on the rotational speed of the device, as proven in this study. The rotational speed impacts the device's wake generation and turbulence mixing.

5. Conclusion

This study aims to compare the wake turbulence produced by two hypothetical actuator cylinders with distinct diameters to that produced by a Savonius turbine design. Additionally, this study compares the wake turbulence produced by the static and dynamic Savonius turbine simulations.

The results indicate that as the diameter of the geometry of the turbine increases, the time taken for the seawater velocity to recover will be longer. Additionally, the geometry of the design has a noticeable influence on the fluid flow over the turbine. For example, the Savonius turbine generates a longer wake owing to fluid fluctuation at the turbine's upstream surface. Using the Savonius turbine design will offer better precision than representing a turbine with a hypothetical actuator cylinder.

When comparing the wake turbulence produced by the static and dynamic Savonius turbine simulations, the Savonius turbine in the dynamic simulation recovered more quickly than in the static simulation. The dynamic simulation's quicker recovery time is due to the 7.5 rad/s rotation velocity. This velocity enables the fluid to flow more readily through the dynamic turbine than in the static turbine, which serves as a barrier to the fluid.

Finally, developing and extracting more renewable energy sources, such as tidal energy, in Malaysia would

reduce fossil fuel dependency and thus mitigate the impact of climate change. Therefore, we highly recommend that more studies focus on expanding the usage of marine renewable energy in Malaysia.

Acknowledgements

The authors gratefully acknowledge the financial support received from the Ministry of Higher Education Malaysia through the Fundamental Research Grant Scheme for Research Acculturation of Early Career Researchers (FRGSRACER) RACER/1/2019/TK07/UNIMAP/1.

Author Contributions: Anas.: Conceptualisation, methodology, supervision, resources, writing—review, editing, Kumaran.: writing—original draft, simulation and validation, Ayu; writing—review, editing, Gisrina.: Conceptualisation, methodology, Lakshuman,: Conceptualisation, methodology. All authors have read and agreed to the published version of the manuscript.

Funding: This research was funded by the Ministry of Higher Education Malaysia through the Fundamental Research Grant Scheme for Research Acculturation of Early Career Researchers (FRGSRACER) RACER/1/2019/TK07/UNIMAP/1.

Conflicts of Interest: Authors declare no conflict of interest.

References

Abdullah, C., Mad Kaidi, H., Sarip, S., & Shafie, N. (2021). Small scale standalone solar and tidal hybrid power system in isolated area. *Renewable Energy Focus*, *39*(00), 59–71. https://doi.org/10.1016/j.ref.2021.07.010

Aliferis, A. D., Bracchi, T., & Hearst, R. J. (2019). *Performance and wake of a Savonius vertical-axis wind turbine under different incoming conditions*. *August 2018*, 1260–1273. https://doi.org/10.1002/we.2358

Alipour, R., Alipour, R., Fardian, F., Koloor, S. S. R., & Petrů, M. (2020). Performance improvement of a new proposed Savonius hydrokinetic turbine: a numerical investigation. *Energy Reports*, *6*, 3051–3066. https://doi.org/10.1016/j.egyr.2020.10.072

Alizadeh, H., Jahangir, M. H., & Ghasempour, R. (2020). CFD-based improvement of Savonius type hydrokinetic turbine using optimized barrier at the low-speed flows. *Ocean Engineering*, *202*(March), 107178. https://doi.org/10.1016/j.oceaneng.2020.107178

Anderson, J., Stelzenmuller, N., Hughes, B., Johnson, C., Taylor, B., Sutanto, L., Mcquaide, E., & Polagye, B. (2011). Capstone Project Report : Design and Manufacture of a Cross-Flow Helical Tidal Turbine. In *University of Washington*.

Azrulhisham, E. A., Jamaluddin, Z. Z., Azri, M. A., & Yusoff, S. B. M. (2018). Potential Evaluation of Vertical Axis Hydrokinetic Turbine Implementation in Equatorial River. *Journal of Physics: Conference Series*, *1072*(1). https://doi.org/10.1088/1742-6596/1072/1/012002

Badrul Salleh, M., Kamaruddin, N. M., & Mohamed-Kassim, Z. (2019). Savonius hydrokinetic turbines for a sustainable river-based energy extraction: A review of the technology and potential applications in Malaysia. *Sustainable Energy Technologies and Assessments*, *36*(July), 100554. https://doi.org/10.1016/j.seta.2019.100554

Bakri, A. (2020). *Numerical Assessment of Vertical Axis Marine Current Turbines Performances in Shallow Water : A Case Study for Malaysia*. Unversiti Malaysia Perlis.

Behrouzi, F., Nakisa, M., Maimun, A., & Ahmed, Y. M. (2016). Renewable energy potential in Malaysia: Hydrokinetic river/marine technology. *Renewable and Sustainable Energy Reviews*, *62*, 1270–1281. https://doi.org/10.1016/j.rser.2016.05.020

Chong, H. Y., & Lam, W. H. (2013). Ocean renewable energy in Malaysia: The potential of the Straits of Malacca. *Renewable and Sustainable Energy Reviews*, *23*, 169–178. https://doi.org/10.1016/j.rser.2013.02.021

Coiro, D. P., Marco, A. De, Nicolosi, F., Melone, S., & Montella, F. (2005). Dynamic Behaviour of the Patented Kobold Tidal Current Turbine: Numerical and Experimental Aspects. *Acta Polytechnica*, *45*(3). https://doi.org/10.14311/718

Daniel, B., & Nicklas, J. (2013). The Development of a Vertical Axis Tidal Current Turbine. In *KTH Industrial Engineering and Management*.

Davis, B. (2001). Ocean energy technology: The Davis Hydro Turbine. In *Refocus* (Vol. 2, Issue 2). https://doi.org/10.1016/S1471-0846(01)80010-X

Energy Commission of Malaysia. (2020). *Malaysia Energy Statistics Handbook*.

Faez Hassan, H., El-Shafie, A., & Karim, O. A. (2012). Tidal current turbines glance at the past and look into future prospects in Malaysia. *Renewable and Sustainable Energy Reviews*, *16*(8), 5707–5717. https://doi.org/10.1016/j.rser.2012.06.016

Hoe, B. C. (2019). The Influence of Tidal Turbine In Array Configuration on The Wake Formation For Shallow Water. In *School of Mechatronic Engineering*. Universiti Malaysia Perlis.

Johnson, B. M. C. (2015). *Computational Fluid Dynamics (CFD) modelling of renewable energy turbine wake interactions* (Issue May). University of Central Lanchashire.

Jung, H., Subban, C. V., McTigue, J. D., Martinez, J. J., Copping, A. E., Osorio, J., Liu, J., & Deng, Z. D. (2022). Extracting energy from ocean thermal and salinity gradients to power unmanned underwater vehicles: State of the art, current limitations, and future outlook. *Renewable and Sustainable Energy Reviews*, *160*(March), 112283. https://doi.org/10.1016/j.rser.2022.112283

Khan, N. I., Iqbal, T., Hinchey, M., & Masek, V. (2009). Performance of Savonius rotor as a water current turbine. *The Journal of Ocean Technology*, *4*(2), 71–83.

Kirke, B. (2019). Hydrokinetic and ultra-low head turbines in rivers: A reality check. *Energy for Sustainable Development*, *52*, 1–10. https://doi.org/10.1016/j.esd.2019.06.002

Kumar, A., Saini, R. P., Saini, G., & Dwivedi, G. (2020). Effect of number of stages on the performance characteristics of modified Savonius hydrokinetic turbine. *Ocean Engineering*, *217*(October), 108090. https://doi.org/10.1016/j.oceaneng.2020.108090

Kuzmin, D., Mierka, O., & Turek, S. (2007). On the implementation of the κ-ε turbulence model in incompressible flow solvers based on a finite element discretisation. *International Journal of Computing Science and Mathematics*, *1*(2–4), 193–206. https://doi.org/10.1504/ijcsm.2007.016531

Lim, Y. S., & Koh, S. L. (2010). Analytical assessments on the potential of harnessing tidal currents for electricity generation in Malaysia. *Renewable Energy*. https://doi.org/10.1016/j.renene.2009.10.016

Magagna, D., & Uihlein, A. (2015). Ocean energy development in Europe: Current status and future perspectives. *International Journal of Marine Energy*. https://doi.org/10.1016/j.ijome.2015.05.001

Mahmoud, N. H., El-Haroun, A. A., Wahba, E., & Nasef, M. H. (2012). An experimental study on improvement of Savonius rotor performance. *Alexandria Engineering Journal*, *51*(1), 19–25. https://doi.org/10.1016/j.aej.2012.07.003

Maldar, N. R., Ng, C. Y., & Oguz, E. (2020). A review of the optimization studies for Savonius turbine considering hydrokinetic applications. *Energy Conversion and Management*, *226*(October), 113495. https://doi.org/10.1016/j.enconman.2020.113495

Maldar, N. R., Ng, C. Y., Patel, M. S., & Oguz, E. (2022). Potential and prospects of hydrokinetic energy in Malaysia: A review.

Sustainable Energy Technologies and Assessments, *52*(PC), 102265. https://doi.org/10.1016/j.seta.2022.102265

Marsh, P., Penesis, I., Nader, J. R., Couzi, C., & Cossu, R. (2021). Assessment of tidal current resources in Clarence Strait, Australia including turbine extraction effects. *Renewable Energy*, *179*, 150–162. https://doi.org/10.1016/j.renene.2021.07.007

Menet, J. L. (2004). A double-step Savonius rotor for local production of electricity: A design study. *Renewable Energy*, *29*(11), 1843–1862. https://doi.org/10.1016/j.renene.2004.02.011

Musa, M. A., Roslan, M. F., Ahmad, M. F., Muzathik, A. M., Mustapa, M. A., Fitriadhy, A., Mohd, M. H., & Rahman, M. A. A. (2020). The influence of ramp shape parameters on performance of overtopping breakwater for energy conversion. *Journal of Marine Science and Engineering*, *8*(11), 1–18. https://doi.org/10.3390/jmse8110875

Neill, S. P., Hemmer, M., Robins, P. E., Griffiths, A., Furnish, A., & Angeloudis, A. (2021). Tidal range resource of Australia. *Renewable Energy*, *170*, 683–692. https://doi.org/10.1016/j.renene.2021.02.035

Priegue, L., & Stoesser, T. (2017). International Journal of Marine Energy The influence of blade roughness on the performance of a vertical axis tidal turbine. *International Journal of Marine Energy*, *17*, 136–146. https://doi.org/10.1016/j.ijome.2017.01.009

Rahman, A., Ibrahim, I., & Rahman, M. T. A. (2019). Assessment of the Malaysian Tidal Stream Energy Resources. *IOP Conference Series: Materials Science and Engineering*, *670*(1). https://doi.org/10.1088/1757-899X/670/1/012025

Roberts, A., Thomas, B., Sewell, P., Khan, Z., Balmain, S., & Gillman, J. (2016). Current tidal power technologies and their suitability for applications in coastal and marine areas. *Journal of Ocean Engineering and Marine Energy*, *2*(2), 227–245. https://doi.org/10.1007/s40722-016-0044-8

Roy, S., & Saha, U. K. (2013). Computational study to assess the influence of overlap ratio on static torque characteristics of a vertical axis wind turbine. *Procedia Engineering*, *51*(NUiCONE 2012), 694–702. https://doi.org/10.1016/j.proeng.2013.01.099

Satrio, D., Utama, I. K. A. P., & Mukhtasor. (2016). Vertical Axis Tidal Current Turbine: Advantages and Challenges Review. *Proceeding of Ocean, Mechanical and Aerospace - Science and Engineering-*, *3*(July), 64–71.

Suhri, G. E., Abdul Rahman, A., Dass, L., Rajendran, K., & Abdul Rahman, A. (2022). Interactions Between Tidal Turbine Wakes: Numerical Study For Shallow Water Application. *Jurnal Teknologi*, *84*(4), 91–101. https://doi.org/https://doi.org/10.11113/jurnalteknologi.v84.17731

Tan, K. W., Kirke, B., & Anyi, M. (2021). Small-scale hydrokinetic turbines for remote community electrification. *Energy for Sustainable Development*, *63*, 41–50. https://doi.org/10.1016/j.esd.2021.05.005

Tawi, K., Yaakob, O., & Sunanto, D. T. (2010). Computer simulation studies on the effect overlap ratio for savonius type vertical axis marine current turbine. *International Journal of Engineering, Transactions A: Basics*, *23*(1), 79–88.

VanZwieten, J. H., Rauchenstein, L. T., & Lee, L. (2017). An assessment of Florida's ocean thermal energy conversion (OTEC) resource. *Renewable and Sustainable Energy Reviews*, *75*(November 2016), 683–691. https://doi.org/10.1016/j.rser.2016.11.043

Yaakob, O. B., Yasser, M., Bin Mazlan, M. N., Jaafar, K. E., & Raja Muda, R. M. (2013). Model testing of an ocean wave energy system for Malaysian sea. *World Applied Sciences Journal*, *22*(5), 667–671. https://doi.org/10.5829/idosi.wasj.2013.22.05.2848

Yaakob, O., Rashid, T. A., & Mukti, M. (n.d.). Prospects for ocean energy in Malaysia. *International Conference on Energy and Environment 2006*.